Chinese Chemical Letters 37 (2026) 111459

Contents lists available at ScienceDirect

Chinese Chemical Letters

journal homepage: www.elsevier.com/locate/cclet

Cyclodextrin-mediated efficient antibody immobilization on upconversion nanoparticles for CKD biomarker sensing *via* luminescent lateral flow assay

Bingyan Wen, Wenjing Zhang, Qi-Wei Zhang*, Yang Tian

Shanghai Key Laboratory of Green Chemistry and Chemical Processes, Department of Chemistry, School of Chemistry and Molecular Engineering, East China Normal University, Shanghai 200241, China

ARTICLE INFO

Article history:
Received 24 December 2024
Revised 11 April 2025
Accepted 13 June 2025
Available online 14 June 2025

Keywords:
Cyclodextrin
Rare-earth
Antibody
Upconversion
Chronic kidney disease
Lateral flow assay

ABSTRACT

Chronic kidney disease (CKD) is a progressive disease characterized by high rates of morbidity and mortality, often leading to various complications. Early home diagnosis and point-of-care prognosis are therefore crucial for monitoring CKD progression and managing patient outcomes. β2-microglobulin (B2M) levels offer a valuable indicator of renal function changes, however, their quantitative detection typically relies on sophisticated and costly laboratory instrumentation. Here, we present a universal and adaptable strategy for efficiently conjugating rare-earth-based nanoparticles with antibodies *via* a carboxymethyl β-cyclodextrin-mediated "self-assembly-followed-by-conjugation" approach. Cyclodextrin modification enhances the rigidity, hydrophilicity, and electrostatic repulsion of nanoparticles, significantly improving their colloidal stability and upconversion luminescence in aqueous solution. Moreover, the ample carboxyl groups on cyclodextrin offer multiple sites for covalent conjugation, resulting in a substantial enhancement in antibody loading capacity and improved immunoaffinity for biomarkers. Employing this methodology, we developed an antibody-conjugated nanoprobe for B2M and fabricated a fluorescent lateral flow strip. Subsequently, image acquisition and data analysis using a smartphone enabled sensitive and quantitative detection of B2M in artificial urine, achieving a detection limit of 2.7 ng/mL. This study provides a versatile strategy for the development of nanoparticle-based colorimetric/luminescent immunoassay probes.

© 2025 Published by Elsevier B.V. on behalf of Chinese Chemical Society and Institute of Materia Medica, Chinese Academy of Medical Sciences.

Chronic kidney disease (CKD) is a progressive condition characterized by structural alterations in the kidneys and a deterioration in renal function due to diverse etiologies [1]. The global prevalence of kidney disease is on the rise, with the World Health Organization identifying it as the eleventh leading cause of death worldwide [2]. However, early-stage CKD frequently presents with vague symptoms, and patients may not experience notable discomfort, leading to delayed diagnosis and treatment [3]. Point-of-care testing (POCT) of biomarkers shows promise for early CKD detection and continuous monitoring to help reduce the global CKD burden [4]. For instance, β2-microglobulin (B2M) could serve as a valuable biomarker for early-stage CKD, which is primarily reabsorbed and metabolized in the proximal renal tubules, maintaining consistent levels in both blood and urine under normal physiological conditions [5,6]. Elevated urinary B2M levels indicate renal dysfunction and damage to the glomerular and tubular structures [7]. Despite the critical importance of these biomarkers, current clinical detection methods, such as radioimmunoassay [8,9], enzyme-linked immunosorbent assay (ELISA) [10], high-performance liquid chromatography (HPLC) and mass spectrometry (MS) [11,12], either involve cumbersome operational procedures or require costly and sophisticated laboratory equipment, hindering real-time home testing. Hence, there is a pressing demand to develop a sensitive, rapid, and user-friendly method for biomarker sensing to facilitate early screening and prognostic management of CKD.

The lateral flow assay (LFA) is a one-step immunoassay technique recognized for its simplicity, rapidity, and cost-effectiveness, rendering it a prevalent technology in POCT [13–15]. Colloidal gold is commonly used as a label in LFA strips due to its economical production and visible detection capabilities. However, colorimetric detection methods often encounter challenges related to a limited signal-to-noise ratio, resulting in reduced sensitivity that confines their applicability to qualitative analyses. From this perspective, fluorophore-based luminescent LFA can offer unique advantages [16,17]. In comparison to traditional organic fluorophores [18–25],

* Corresponding author.
E-mail address: qwzhang@chem.ecnu.edu.cn (Q.-W. Zhang).

https://doi.org/10.1016/j.cclet.2025.111459
1001-8417/© 2025 Published by Elsevier B.V. on behalf of Chinese Chemical Society and Institute of Materia Medica, Chinese Academy of Medical Sciences.

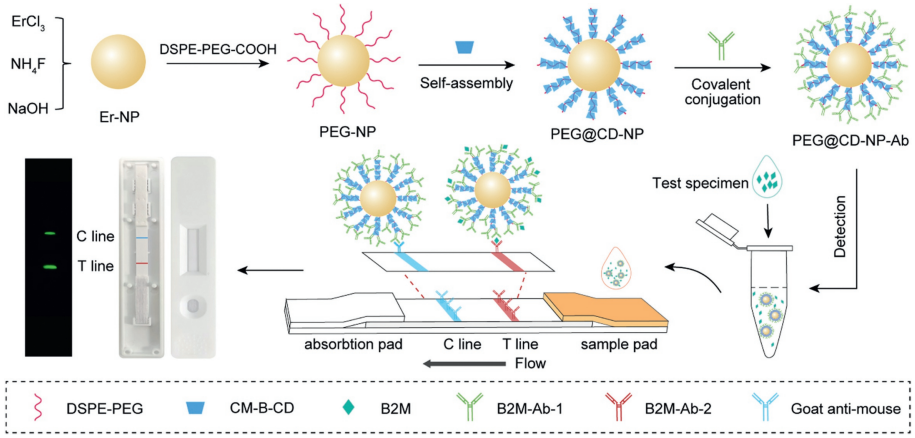


Fig. 1. Schematic illustration of the cyclodextrin-mediated antibody immobilization on upconversion nanoparticles for CKD biomarker sensing *via* quantitative luminescent lateral flow assay.

lanthanide-activated upconversion nanoparticles (UCNPs) possess the ability to convert longer-wavelength (near-infrared, NIR) irradiations into shorter-wavelength (visible) emissions, along with superior photochemical stability, prolonged luminescence lifetime, and minimal background signal, leading to widespread applications in bioimaging and theranostics [26–29]. Nevertheless, UCNPs are typically synthesized in organic solvents containing oleic acid (OA), resulting in poor aqueous dispersibility and colloidal stability. Furthermore, as a potential fluorescent label for LFA, enhancing the loading capacity of antibodies on the nanoparticle surface to improve immunoaffinity for biomarkers remains a significant challenge.

Herein, we report a novel cyclodextrin-mediated "self-assembly-followed-by-conjugation" strategy for UCNP-antibody conjugation. Initially, the UCNPs β-$NaYF_4$:Yb/Er (Er-NPs) were synthesized and coated with amphiphilic ligands (DSPE-PEG-COOH), which were subsequently self-assembled with carboxymethyl-β-cyclodextrin (CM-B-CD) *via* host-guest interactions between the polyethylene glycol (PEG) chains and the cavity of CM-B-CD. This process resulted in the formation of a polyseudorotaxane-type structure on the UCNP surface [30,31], generating PEG@CD-NPs. The incorporation of CM-B-CD led to a significant enhancement in the hydrophilicity, negative charge, and rigidity of the UCNPs' surface ligands, thereby improving the dispersibility, luminescence intensity, and colloidal stability of the nanoparticles in aqueous media. Furthermore, CM-B-CD also provided abundant carboxyl groups for covalent conjugation with amines on antibody molecules, markedly increasing the loading capacity of antibodies and consequently enhancing the immunoaffinity of the nanoprobes towards the target biomarker. By employing this strategy and utilizing B2M as a representative biomarker for CKD, we constructed a LFA strip as a proof-of-concept (Fig. 1). Through the integration of smartphone-based image acquisition and analysis applications, we successfully achieved rapid, sensitive, and quantitative detection of B2M concentration in samples.

Firstly, using oleic acid as the surface ligand, we successfully synthesized monodispersed nanoparticles (designated as Er-NPs) comprising Yb as the sensitizer and Er as the activator, with a composition of $NaYF_4$: 20 % Yb, 2 % Er, *via* a modified solvothermal reaction (detailed in Supporting information). As depicted in Fig. 2a(i), transmission electron microscopy (TEM) images revealed that the synthesized nanoparticles exhibited uniform hexagonal spheres with an average diameter of approximately 80 nm. The powder X-ray diffraction (XRD) patterns indicated that the diffraction peaks of the synthesized nanoparticles matched well with those of the standard hexagonal phase $NaYF_4$ (JCPDS: 16–0334) (Fig. 2b). Moreover, energy dispersive X-ray spectroscopy (EDS) mapping further confirmed the homogeneous distribution of Na, Y, F, Yb and Er elements within the nanoparticles (Fig. 2c). Collectively, these results unequivocally demonstrated the successful synthesis of Er-NPs.

Next, a layer of amphiphilic polymer DSPE-PEG-COOH was applied to the surface of Er-NPs, thereby converting the hydrophobic oleic acid layer into a relatively hydrophilic surface covered with PEG chains, resulting in the formation of new nanoparticles designated as PEG-NPs (Fig. 1). Subsequently, CM-B-CD was introduced to further modify the surface of the PEG-NPs. Ahead of that, we conducted initial verification of the interactions between CM-B-CD and DSPE-PEG-COOH using two-dimensional NOESY nuclear magnetic resonance (2D NOESY NMR). As shown in Fig. 2d, clear nuclear Overhauser effect (NOE) between the methylene protons of PEG chain and the protons from the cavity of cyclodextrin were observed, indicating the spatial proximity between them, and demonstrating the host-guest self-assembly of CM-B-CD with PEG chain in the aqueous phase [32–35]. Leveraging this feature, the incorporation of CM-B-CD resulted in a cyclodextrin layer with polypseudorotaxane-type structure covering the surface of PEG-NPs, leading to the creation of enhanced hydrophilic nanoparticles referred to as PEG@CD-NPs (Fig. 1). TEM image in Fig. 2a(iii) displayed a superficial layer of ~3.5 nm thick on the surface of the nanoparticles post the CM-B-CD modification. In contrast, nanoparticles modified solely with DSPE-PEG-COOH chains did not exhibit this phenomenon (Fig. 2a(ii)). Furthermore, Fourier-transform infrared spectroscopy (FT-IR) revealed characteristic peaks at 1103 cm^{-1} and 1730 cm^{-1} attributed to C–O and C=O stretching vibrations, which proved that the PEG-NPs has been successfully constructed. A comparison between PEG-NPs and PEG@CD-NPs showed a shift in the characteristic peak at 1683 cm^{-1} attributed to C=O stretching vibration and the emergence of a new peak at 3400 cm^{-1} attributed to O–H stretching vibration due to the self-assembly of CM-B-CD on PEG@CD-NPs (Fig. 2e) [36,37]. Further insights into the evolution of surface ligands on the nanoparticles were obtained from XRD experiments. As shown in Fig. 2f, compared to the initial Er-NPs, PEG-NPs showed a weak diffraction peak at 21.62°, which can be attributed to the PEG layer on the surface. However, post modification with CM-B-CD, the diffraction peak of the surface ligand DSPE-PEG-COOH shifted to 21.42° with increased intensity, indicating its host-guest interaction with cyclodextrin [37,38]. Additionally, dynamic light scattering (DLS) experiments visually depicted changes in particle size due to the presence of different surface ligands on the nanoparticles, particularly with the addition of cyclodextrin which led to a more significant increase in particle size attributable to the

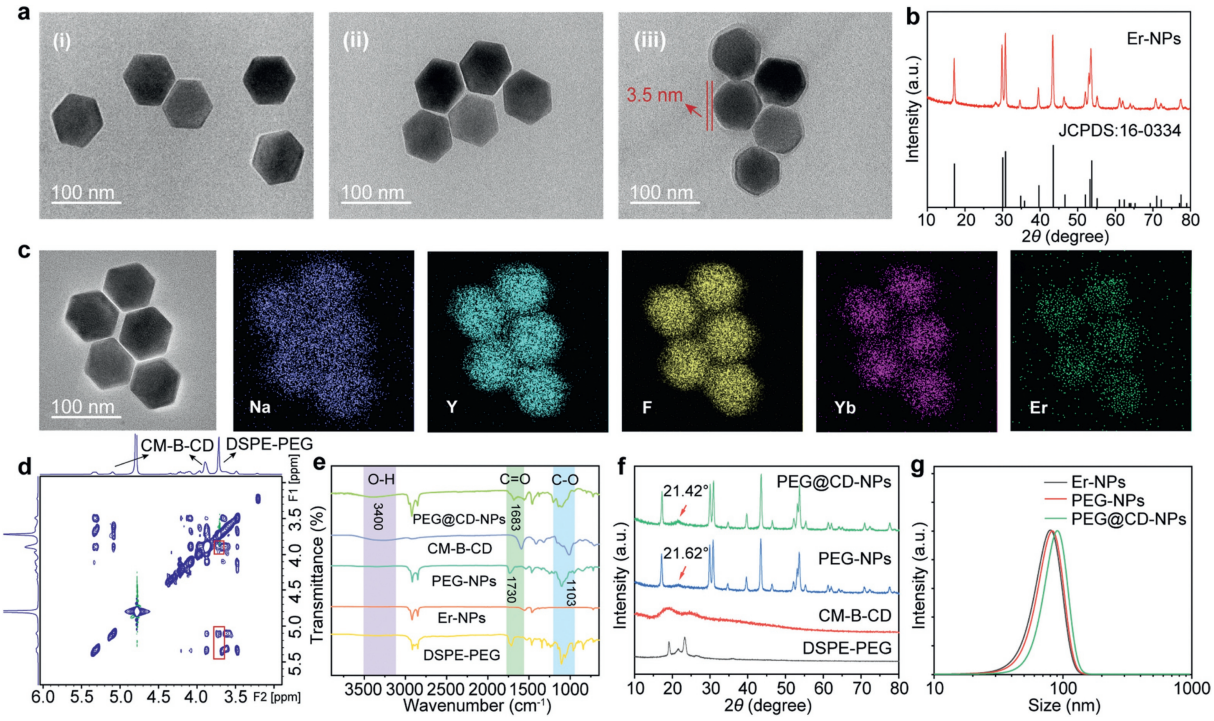


Fig. 2. (a) TEM images of Er-NPs (i), PEG-NPs (ii), and PEG@CD-NPs (iii). (b) Comparison between the experimental X-ray diffraction (XRD) pattern (top) and the standard hexagonal phase $NaYF_4$ XRD pattern (JCPDS: 16–0334) (bottom) of the Er-NPs. (c) TEM image and corresponding EDS element mapping images of the Er-NPs. (d) 2D NOESY NMR spectra of the mixture of DSPE-PEG-COOH and CM-B-CD. FT-IR spectra (e) and XRD patterns (f) of Er-NPs with different surface modifications. (g) Size distributions of Er-NPs, PEG-NPs and PEG@CD-NPs determined through DLS experiments.

enhanced rigidity of the surface ligands (Fig. 2g). Taken together, the evidence presented clearly demonstrated the self-assembly of cyclodextrin on the surface of rare-earth nanoparticles and the successful construction of PEG@CD-NPs.

Afterwards, the physicochemical properties of the synthesized nanoparticles with different ligands modifications were thoroughly characterized. As a potential biological detection indicator, good aqueous dispersibility is essential. However, due to the hydrophobic oleic acid ligand coating on the surface of the initially prepared Er-NPs, their water solubility is poor. Scanning electron microscopy (SEM) images clearly showed the large-scale aggregates of Er-NPs in the aqueous phase (Fig. 3a), which also resulted in upconversion luminescence (UCL) quenching (Fig. 3d(i)). Subsequent modification with DSPE-PEG-COOH significantly improved water solubility, as observed through SEM imaging displaying uniform dispersion in the aqueous phase (Fig. 3b). Besides, due to the hydrophobic cavities in the DSPE-PEG chain coating effectively isolating the UCNP core from water molecules with high vibrational energy, the modified nanoparticles exhibit a reduced water quenching effect, thereby preserving the UCL performance. (Fig. 3d(ii)). Furthermore, the CM-B-CD-assembled nanoparticles (PEG@CD-NPs) exhibited superior monodispersity (Fig. 3c). The cyclodextrin layer on the surface of PEG@CD-NPs can also effectively trap water molecules via hydrogen-bond networks, which may further reduce the quenching effect of surface water, thereby better protecting the luminescent core and establishing them as excellent luminescent indicators in aqueous systems (Fig. 3d(iii)) [39,40].

The enhancement dispersibility and colloidal stability in water due to cyclodextrin coating can also be observed macroscopically. As shown in Fig. 3e, both PEG-NPs and PEG@CD-NPs were evenly dispersed in water initially. However, after standing for 15 days, PEG-NPs showed significant stratification, indicating their aggregation settlement. In contrast, PEG@CD-NPs remained well dispersed, showcasing the crucial role of cyclodextrin modification in enhanc-

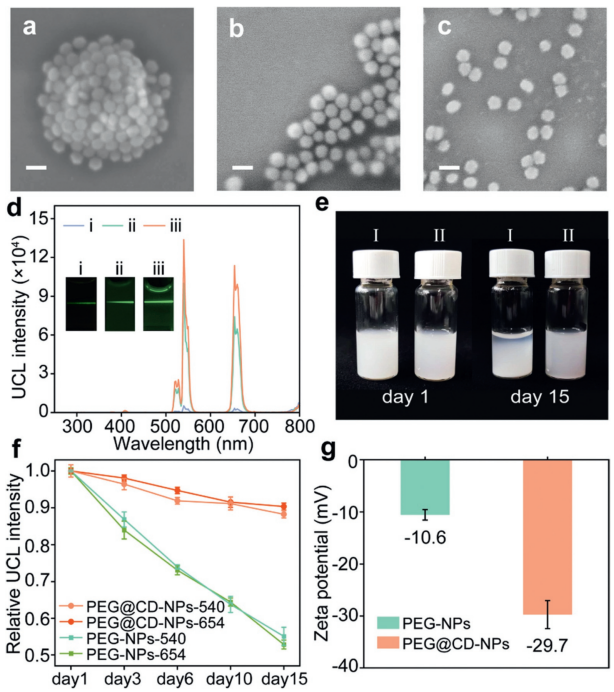


Fig. 3. SEM images of Er-NPs (a), PEG-NPs (b), and PEG@CD-NPs (c) (scale bar, 100 nm). (d) Upconversion luminescence spectra of the different nanoparticles, with insets of their upconversion luminescence images (excited at 980 nm, where i, ii, iii represent the Er-NPs, PEG-NPs, and PEG@CD-NPs, respectively). (e) Photographs of the aqueous dispersions of PEG-NPs (I) and PEG@CD-NPs (II) on day 1 and day 15. (f) Luminescence intensity of the supernatant samples from the aqueous samples of PEG-NPs and PEG@CD-NPs at 540 nm and 654 nm as a function of standing time. (g) Zeta potential values of the different nanoparticles.

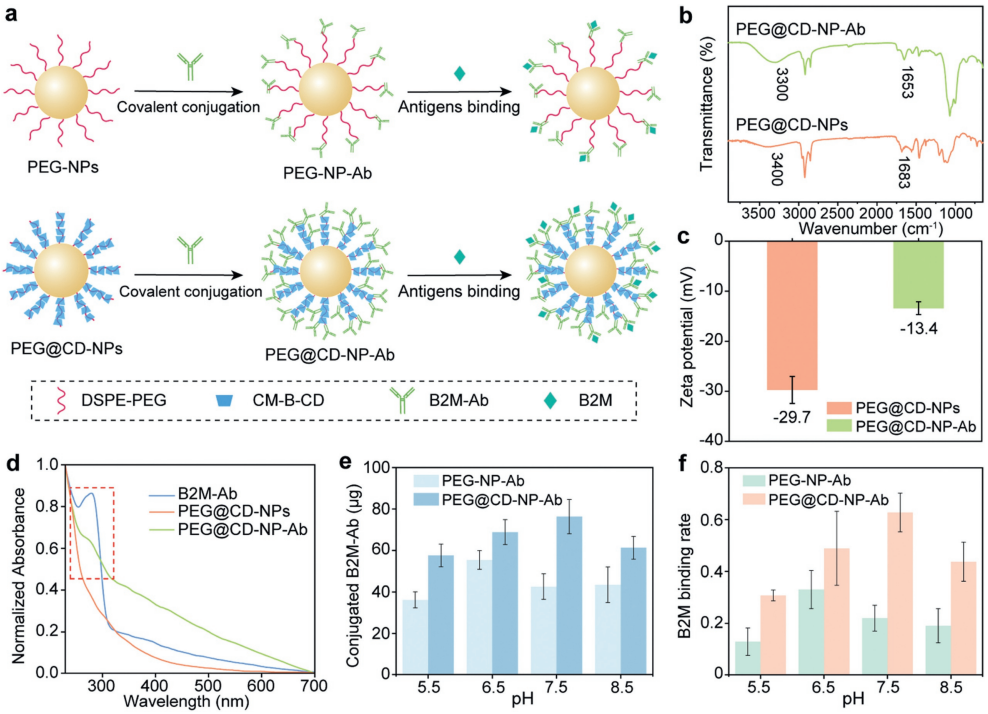


Fig. 4. (a) Schematic representation of the preparation process for PEG-NP-Ab and PEG@CD-NP-Ab, along with their binding affinity to B2M. (b) FT-IR spectra, (c) zeta potential and (d) UV-visible absorption spectra of PEG@CD-NP and PEG@CD-NP-Ab. (e) Assessment of the conjugated antibodies on PEG-NP-Ab and PEG@CD-NP-Ab fabricated under varying pH conditions. (f) Binding rates of PEG-NP-Ab and PEG@CD-NP-Ab nanoprobes produced under different pH conditions towards B2M.

ing aqueous colloidal stability. The colloidal stability of PEG@CD-NPs in water could also be confirmed by luminescent measurement. As shown in Fig. 3f, their upconversion luminescence intensity at two characteristic emission wavelengths (540 nm and 654 nm) were recorded by intermittently sampling from the upper layer of the dispersion of these two samples. The results demonstrated that with prolonged standing time, the luminescent intensity of PEG-NPs sample rapidly decreased, reaching only ~50 % of the initial value after 15 days. In contrast, the luminescent intensity decrease of PEG@CD-NPs is much slower, retaining over 90 % of the initial intensity after 15 days. This comparison clearly illustrated the important role of cyclodextrin modification in enhancing the aqueous colloidal stability of the synthesized rare-earth nanoparticles, which not only attributed to the improved water solubility due to the abundant cyclodextrin coverage but also related to the increased surface charge caused by the numerous carboxyl groups on CM-B-CD. As shown in Fig. 3g, the zeta potential of PEG-NPs measured in the aqueous solution is only −10.6 mV, whereas that of the PEG@CD-NPs reached −29.7 mV, indicating the enhanced electrostatic repulsion force, and approaching the stability threshold for colloids (~30 mV). Therefore, the above results demonstrated that PEG@CD-NPs exhibit superior hydrophilicity, stronger luminescence, and enhanced colloidal stability, laying a solid foundation for the development of high-performance nanoprobes for biosensing.

To develop specific probes for the CKD biomarker B2M, we further conjugated the monoclonal antibody B2M-antibody (B2M-Ab-1, clone 15F6) to the as-prepared luminescent indicator PEG@CD-NPs using EDC/sulfo-NHS-mediated amidation, yielding the antibody-conjugated nanoprobe denoted as PEG@CD-NP-Ab (Fig. 4a). The successful formation of covalent bonds between the luminescent nanoparticles and the antibodies was first characterized by FT-IR spectroscopy. A comparison between the FTIR spectra of PEG@CD-NPs and PEG@CD-NP-Ab (Fig. 4b) revealed a shift in the C=O stretching vibration peak from 1683 cm^{-1} to 1653 cm^{-1}. Additionally, a distinct strong broad peak at 3300 cm^{-1} emerged, assignable to the characteristic N–H stretching vibration peak. These spectral changes can be attributed to the formation of amide bonds between the nanoparticles and the antibodies [41]. On the other hand, the zeta potential of the nanoparticles significantly decreased due to the consumption of free carboxyl groups on cyclodextrin (Fig. 4c). Furthermore, UV–visible absorption spectroscopy unveiled a new absorption peak at 280 nm for PEG@CD-NP-Ab compared to PEG@CD-NPs, which was attributed to protein absorption, confirming the successful conjugation of antibodies to the nanoparticle surface (Fig. 4d) [42]. Utilizing the same methodology, a control probe named PEG-NP-Ab was prepared as well by conjugating B2M-antibody with PEG-NPs lacking cyclodextrin modification (Fig. 4a). The successful construction of PEG-NP-Ab was validated, as depicted in Fig. S1 in Supporting information.

Considering the significant pH influence on the rate and yield of the condensation reaction between sulfo-NHS-activated carboxyl and primary amines, we proceeded to optimize the pH conditions for the covalent conjugation of nanoparticles with antibodies. The average amounts of conjugated antibodies on nanoparticles were utilized to assess the efficiency of coupling (calculated based on the discrepancy between the initial amount of input antibody and the residual free antibody post-reaction). As shown in Fig. 4e, within the experimental pH range (5.5–8.5), the antibody coupling levels of PEG@CD-NPs surpassed those of PEG-NPs, reaching the highest coupling efficiency at pH 7.5. Moreover, the increased antibody coupling amount also led to a higher binding rate of the antigen (B2M) to the nanoprobe PEG@CD-NP-Ab compared to PEG-NP-Ab under identical conditions (Fig. 4f). These findings indicated that the multi-carboxylated cyclodextrin modification facilitated the provision of more reaction sites for coupling with primary amines in the antibody, thereby enhancing antibody loading and improving antigen binding performance.

After optimizing the synthesis conditions and confirming the superior performance of PEG@CD-NP-Ab, it was employed as a

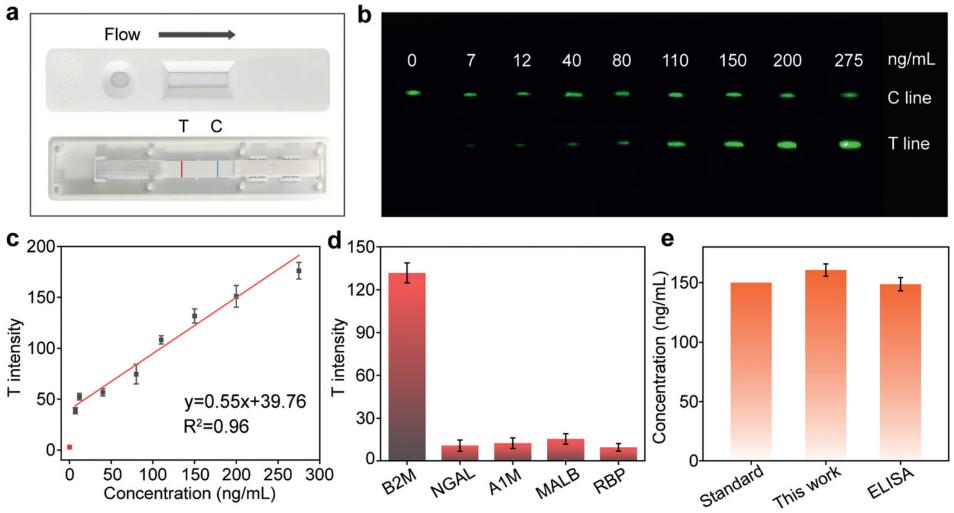


Fig. 5. (a) Photographs of the LFA test strip, where the red line indicates the test line (T line) and the blue line indicates the control line (C line). (b) Upconversion luminescence images of PEG@CD-NP-Ab nanoprobe-based LFA strips with different concentrations of B2M standard solutions under 980 nm laser irradiation. (c) Linear relationships between the signal intensity at the T lines and the concentrations of B2M (mean ± SD, $n = 3$). (d) Selectivity evaluation of the developed LFA strips towards common CKD biomarkers at their physiological levels, from left to right: 150 ng/mL, 7.2 ng/mL, 9 μg/mL, 15 μg/mL, and 0.5 μg/mL (mean ± SD, $n = 3$). (e) Accuracy assessment of the developed LFA strips for the detection of standard B2M samples in artificial urine.

luminescent nanoprobe for the development of luminescent LFA strips aimed at in vitro detection of B2M (Fig. 5a). Practically, a test sample was mixed with the nanoprobe solution for approximately 5 min, after which the mixture was dispensed onto the sample pad of the test strip. In the event that the test sample contains the target antigen B2M, it will initially bind to PEG@CD-NP-Ab to create the nanoprobe-antigen conjugate. Subsequently, this conjugate will be transported to the test line (T line) on the sample pad through capillary force, forming a sandwich configuration with the second antibody (B2M-Ab-2, Clone 19F9) immobilized in the T line, thereby generating a sensing signal. While the excess free nanoprobes would continue to flow forward and be trapped by the goat anti-mouse antibody on the control line (C line). Subsequently, the LFA strips can be illuminated under 980 nm laser irradiation, and the UCL signal can be imaged using a smartphone and then analyze using smartphone applications like a Color Picker, to quantify the signal intensity (I) based on the RGB values within the image. Specifically, the signal intensity can be quantified using the formula $I = 0.3R + 0.59G + 0.11B$ [43]. Consequently, the presence of solely signal on the C line indicates the absence of detectable B2M in the sample (negative result), while the luminescence signals present on both the C line and T line signify the presence of B2M in the sample (positive result), as schemed in Fig. 1.

Fig. 5b showed the upconversion luminescence images of the LFA strips reacted with B2M samples at various concentrations ranging from 0 to 275 ng/mL. The outcomes indicated that the luminescence signal intensities of T line were positively correlated with the concentration of B2M, with the lowest observable luminescence signal at 7 ng/mL. Furthermore, by plotting the intensity values on the T lines against the concentrations of B2M samples, a good linear relationship could be fitted within the B2M concentrations ranging from 7 ng/mL to 275 ng/mL, and the limit of detection (LOD) was calculated to be 2.7 ng/mL (S/N = 3), which has met the requirements for detection, as the normal clinical threshold is 200 ng/mL [44], affirming the capability of quantitatively detecting B2M using this nanoprobe-based luminescent LFA strips (Fig. 5c). Then, recovery tests were conducted to evaluate the accuracy and detection stability of the LFA strips. As shown in Table S1 (Supporting Information), the average recovery values of this method were 86 % – 106.3 %, with relative standard deviations (RSD) of 3.3 % to 10.5 %, indicating good accuracy and detection stability for the developed test strips. Subsequently, to validate the specificity of the developed strips, four other commonly used CKD biomarkers, such as neutrophil gelatinase-associated lipocalin (NGAL), α1-microglobulin (A1M), microalbumin (MALB), and retinol-binding protein (RBP), were evaluated as interferents at their physiological concentrations. The luminescence intensities at the T lines for the aforementioned samples were presented in Fig. 5d, wherein only B2M elicited a significant signal intensity, while the signal from the other interferents was nearly negligible, underscoring the exceptional specificity towards B2M. Finally, to validate the feasibility and reliability of the developed LFA strips for practical application in biological samples, a standard B2M sample (150 ng/mL) was prepared in artificial urine. Subsequently, both the prepared LFA strip and a commercial ELISA kit were employed to detect the sample, in which the former exhibited a satisfactory average deviation of +6.7 % compared to the standard concentration (Fig. 5e). Therefore, the PEG@CD-NP-Ab nanoprobe-based luminescence LFA strip hold significant practical value in our daily lives, particularly in the context of chronic disease detection, owing to its rapid detection speed and ease of operation.

In summary, this study presents a unique technique involving the cyclodextrin-mediated surface modification of rare-earth nanoparticles and their covalent conjugation with antibodies. The host-guest self-assembly of cyclodextrin and PEG ligands on the surface of rare-earth nanoparticles leads to a significant enhancement of the solubility and colloidal stability, along with improved upconversion luminescence performance in water, thus ensuring their promising application as luminescent indicators in biological samples. Furthermore, the presence of abundant carboxyl groups on cyclodextrin provide ample covalent binding sites, resulting in a substantial increase in antibody loading capacity and consequently enhancing the affinity of the nanoprobes towards target biomarkers. As a proof-of-concept, a LFA strip was constructed utilizing the PEG@CD-NP-Ab nanoprobe for the quantitative detection of a CKD biomarker (B2M), showing excellent specificity, sensitivity, and accuracy, which has reached the detection level of reported POC methods [45]. Although this work still has certain limitations, such as the step-by-step detection mode increasing operational complexity and detection time to some extent, and the approach of calculating signal intensity based on RGB values showing gaps in precision and accuracy compared to direct fluorescence

intensity measurement, future research could further optimize signal acquisition strategies, and develop an all-in-one portable detection device to enhance detection efficiency. In general, this work not only introduces a rare-earth-based luminescent nanoprobe for efficient and rapid LFA testing of CKD biomarkers but also demonstrates the simplicity and versatility of the cyclodextrin-mediated "self-assembly-followed-by-conjugation" methodology, which can be readily applied to the development of various nanoparticle-based immunoassays.

Declaration of competing interest

The authors declare that they have no known competing financial interests or personal relationships that could have appeared to influence the work reported in this paper.

CRediT authorship contribution statement

Bingyan Wen: Data curation, Investigation, Methodology, Writing – original draft. **Wenjing Zhang:** Investigation. **Qi-Wei Zhang:** Conceptualization, Data curation, Funding acquisition, Project administration, Writing – review & editing. **Yang Tian:** Funding acquisition, Project administration.

Acknowledgments

This research was made possible as a result of generous grants from the National Key Research & Development Program of China (No. 2022YFF0710000), National Natural Science Foundation of China (NSFC, Nos. 22322405, 22274055, and 22393930), Shanghai Pilot Program for Basic Research (No. TQ20240206), and the Fundamental Research Funds for the Central Universities.

Supplementary materials

Supplementary material associated with this article can be found, in the online version, at doi:10.1016/j.cclet.2025.111459.

References

[1] A. Francis, M.N. Harhay, A.C.M. Ong, et al., Nat. Rev. Nephrol. 20 (2024) 473–485.
[2] M. Naghavi, K.L. Ong, A. Aali, et al., The Lancet 403 (2024) 2100–2132.
[3] K. Kalantar-Zadeh, T.H. Jafar, D. Nitsch, et al., The Lancet 398 (2021) 786–802.
[4] Z. Zhu, X. Chen, H. Liao, et al., Aggregate 5 (2024) e526.
[5] T. Miyata, M. Jadoul, K. Kurokawa, C. Van Ypersele de Strihou, J. Am. Soc. Nephrol. 9 (1998) 1723–1735.
[6] J. Carbayo, Ú. Verdalles, F. Díaz-Crespo, et al., Clin. Kidney J. 17 (2024) sfae146.
[7] S. Apakkan Aksun, D. Özmen, B. Özmen, et al., Exp. Clin. Endocrinol. Diabetes 112 (2004) 195–200.
[8] H.M. Kantarjian, T. Smith, E. Estey, et al., Am. J. Med. 93 (1992) 599–604.
[9] J.P. Gosling, Clin. Chem. 36 (1990) 1408–1427.
[10] P.A. Tomlinson, R.N. Dalton, C. Turner, C. Chantler, Clin. Chim. Acta 192 (1990) 99–106.
[11] K.A. Tubbs, D. Nedelkov, R.W. Nelson, Anal. Biochem. 289 (2001) 26–35.
[12] C.T. Chang, H.Y. Liao, W.H. Huang, et al., Clin. Chim. Acta 440 (2015) 115–122.
[13] Z. Zhang, P. Ma, R. Ahmed, et al., Adv. Mater. 34 (2022) 2103646.
[14] L. Roy, P. Buragohain, V. Borse, Biosens. Bioelectron.: X 10 (2022) 100098.
[15] G. Guo, T. Zhao, R. Sun, et al., Chin. Chem. Lett. 35 (2024) 109198.
[16] D. Lou, L. Fan, T. Jiang, Y. Zhang, View 3 (2022) 20200125.
[17] S. Kim, Y. Ahn, Y. Bae, et al., Biosens. Bioelectron. 213 (2022) 114441.
[18] Y. Han, L. Mao, Q.W. Zhang, Y. Tian, J. Am. Chem. Soc. 145 (2023) 23832–23841.
[19] L. Mao, Y. Han, Q.W. Zhang, Y. Tian, Nat. Commun. 14 (2023) 1419.
[20] S. Li, R. Chang, L. Zhao, et al., Nat. Commun. 14 (2023) 5227.
[21] Y. Song, X. Tong, Y. Han, Q.W. Zhang, Aggregate 6 (2025) e680.
[22] X. Wang, X. Yang, G. Jiang, et al., Angew. Chem. Int. Ed. 63 (2024) e202404142.
[23] X. Gu, X. Wang, W. Cai, et al., ACS Sens. 9 (2024) 3387–3393.
[24] Z. Gong, Z. Liu, Z. Zhang, et al., CCS Chem. 4 (2021) 2020–2030.
[25] Q. Xu, X. Lin, L. Ma, et al., Chin. Chem. Lett. 33 (2022) 2965–2968.
[26] W. He, M. Wang, P. Cheng, et al., Trends. Anaytl. Chem. 173 (2024) 117641.
[27] Y. Liu, X. Zhu, Z. Wei, et al., Adv. Mater. 33 (2021) 2008615.
[28] S. Wen, J. Zhou, P.J. Schuck, et al., Nat. Photonics 13 (2019) 828–838.
[29] Y. Gu, Z. Guo, W. Yuan, et al., Nat. Photonics 13 (2019) 525–531.
[30] D.H. Qu, Q.C. Wang, Q.W. Zhang, et al., Chem. Rev. 115 (2015) 7543–7588.
[31] Q.W. Zhang, H. Tian, Angew. Chem. Int. Ed. 53 (2014) 10582–10584.
[32] Q.W. Zhang, J. Zajíček, B.D. Smith, Org. Lett. 20 (2018) 2096–2099.
[33] S. Stoffel, Q.W. Zhang, D.H. Li, et al., J. Am. Chem. Soc. 142 (2020) 7413–7424.
[34] D. Li, Y. Han, Y. Jiang, et al., ACS Appl. Mater. Interfaces 14 (2022) 1807–1816.
[35] Q.W. Zhang, H.J.A.A.W. Elemans, P. White, R.J.M. Nolte, Chem. Commun. 54 (2018) 5586–5589.
[36] B. Liu, J. Zhang, C. Chen, et al., J. Agric. Food. Chem. 69 (2021) 6981–6988.
[37] H. Lan, T. Huang, J. Xiao, et al., J. Cell. Mol. Med. 25 (2021) 561–574.
[38] Y. Ke, X. Zhang, C. Liu, et al., Mater. Sci. Eng. C 99 (2019) 159–170.
[39] S. Wilhelm, M. Kaiser, C. Würth, et al., Nanoscale 7 (2015) 1403–1410.
[40] Y. Wang, Z. Li, Z. Liu, Prog. Chem. 28 (2016) 617–627.
[41] X. Sun, X. Dai, S. Ling, et al., Analyst 148 (2023) 2717–2724.
[42] H.D. Wang, C.H. Niu, Q. Yang, I. Badea, Nanotechnology 22 (2011) 145703.
[43] J.Y. Yue, L.P. Song, Y.T. Wang, et al., Anal. Chem. 94 (2022) 14419–14425.
[44] C.P. Argyropoulos, S.S. Chen, Y.H. Ng, et al., Front. Med. 4 (2017) 73.
[45] S. Maity, S. Ghosh, T. Bhuyan, D. Das, D. Bandyopadhyay, ACS Sustain. Chem. Eng. 8 (2020) 9268–9276.